Low-Temperature Dielectric Anisotropy Driven by an Antiferroelectric Mode in $SrTiO_3$

Blai Casals,[1] Andrea Schiaffino,[1] Arianna Casiraghi,[2] Sampo J. Hämäläinen,[2] Diego López González,[2] Sebastiaan van Dijken,[2] Massimiliano Stengel,[1,3] and Gervasi Herranz[1]

[1]*Institut de Ciència de Materials de Barcelona (ICMAB-CSIC), Campus UAB, 08193 Bellaterra, Catalonia, Spain*
[2]*NanoSpin, Department of Applied Physics, Aalto University School of Science, P.O. Box 15100, FI-00076 Aalto, Finland*
[3]*ICREA–Institució Catalana de Recerca i Estudis Avançats, Passeig Lluís Companys, 23, 08010 Barcelona, Catalonia, Spain*

(Received 21 September 2017; revised manuscript received 9 January 2018; published 25 May 2018)

Strontium titanate ($SrTiO_3$) is the quintessential material for oxide electronics. One of its hallmark features is the transition, driven by antiferrodistortive (AFD) lattice modes, from a cubic to a ferroelastic low-temperature phase. Here we investigate the evolution of the ferroelastic twin walls upon application of an electric field. Remarkably, we find that the dielectric anisotropy of tetragonal $SrTiO_3$, rather than the intrinsic domain wall polarity, is the main driving force for the motion of the twins. Based on a combined first-principles and Landau-theory analysis, we show that such anisotropy is dominated by a trilinear coupling between the polarization, the AFD lattice tilts, and a previously overlooked antiferroelectric (AFE) mode. We identify the latter AFE phonon with the so-called "*R* mode" at ~440 cm^{-1}, which was previously detected in IR experiments, but whose microscopic nature was unknown.

DOI: 10.1103/PhysRevLett.120.217601

Because of its attractive physical properties, strontium titanate ($SrTiO_3$) has long captured the attention of condensed matter physicists, becoming an iconic material among oxide perovskites. At room temperature $SrTiO_3$ crystallizes in the cubic perovskite structure with space group $Pm3m$ [1]. Yet, at $T \sim 105$ K, $SrTiO_3$ crystals undergo a ferroelastic transition, to a tetragonal phase ($I4/mcm$ space group, $c/a \approx 1.0005$) [2,3]. Such transition is driven by an antiferrodistortive (AFD) lattice mode, with neighboring TiO_6 octahedra rotating in antiphase along the [001] axis. [4,5] The most obvious manifestation of tetragonality is the anisotropy of the dielectric constant [6,7], which is responsible for the observed birefringence [8]. Recently, ferroelastic domain formation was shown [9–11] to strongly influence other electronic phenomena in $SrTiO_3$, e.g., superconductivity [12] or two-dimensional electron gases [13–15]. The ability of controlling the electronic degrees of freedom by altering the ferroelastic domain structure provides, in principle, a tantalizing opportunity for new device concepts. To explore this route, however, one first needs to understand whether (and how) the ferroelastic degrees of freedom can be harnessed via a suitable external field. As the ferroelastic domain walls have recently been shown to be polar [16–22], it is reasonable to expect that they will respond to an electrical bias. A detailed study on the evolution of the domain wall topology upon application of a voltage is currently missing, leaving the above question largely unanswered.

Here we use optical microscopy to image ferroelastic twins under an applied electric field, as done previously (at zero field) in $SrTiO_3$ single crystals [23] and heterointerfaces [10,24]. We find that the domain structure undergoes dramatic changes with the applied external bias. Remarkably, however, such changes cannot be explained by invoking the intrinsic polarity of the walls; instead, we interpret our observations as a consequence of the higher polarizability of ferroelastic domains in the plane normal to the tetragonal axis. Based on our first-principles calculations, we find that such a dielectric anisotropy is largely determined by a trilinear coupling between the polarization, the tilts, and a previously unreported antiferroelectric (AFE) mode. Interestingly, by means of the same mechanism, the AFE mode, whose predicted frequency is ~440 cm^{-1}, becomes IR active below the transition temperature. This allows us to identify it with the "*R* mode," which was reported at precisely the same frequency in earlier spectroscopic studies [25–27], but whose lattice representation was formerly unknown.

Figure 1(a) shows schematically the two types of twin structures that are visible at the surface of a (001)-oriented $SrTiO_3$ crystal. First, we have $\{a\}$ and $\{c\}$ domains, in which the elongated axes are in plane and out of plane, respectively. Second, $\{a_1\}$ and $\{a_2\}$ domains denote $\{a\}$ domains having the elongated axis along orthogonal directions within the plane. Since $\{a, c\}$ domains corrugate the surface, their emergence is revealed by optical reflection microscopy as a striped contrast along in-plane [100] and [010] directions [Fig. 1(c)]. Conversely, $\{a_1, a_2\}$ domains do not corrugate the surface, and they cannot be detected in this way. Interestingly, our experiments reveal that $\{a, c\}$ regions recede with the application of an electric field [Fig. 1(d)]. The recession of $\{a, c\}$ regions is substantiated by constructing an image as the difference of the data recorded at $V = +200$ V and $V = 0$ V, which highlights the area where $\{a, c\}$ domains recede [Fig. 1(e)].

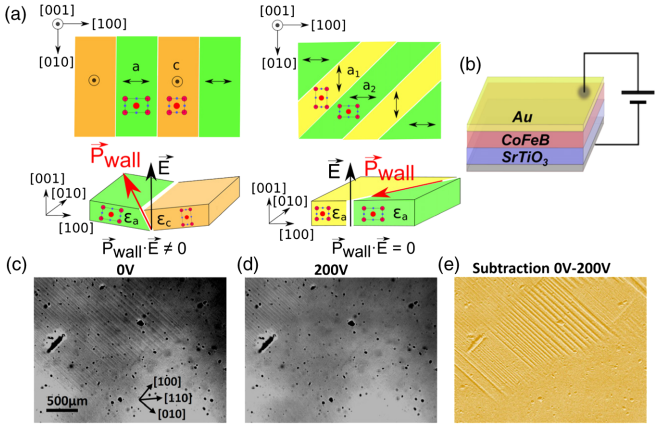

FIG. 1. (a) Schematic representation of ferroelastic twins in $SrTiO_3$ in the tetragonal phase. (b) Illustration of the applied electric field configuration in the sample. Panels (c) and (d) show, respectively, optical images measured at $T = 8$ K and $V = 0$ V and $V = +200$ V. In-plane crystal directions are indicated in (c). At zero field, stripes along [010] indicate the presence of $\{a, c\}$ domains. After applying a voltage $V = +200$ V, the $\{a, c\}$ domains recede. The image in (e) is obtained by the subtraction of the images taken at $V = 0$ V and $V = +200$ V. The large striped area indicates the region were $\{a, c\}$ domains are suppressed by the electric field.

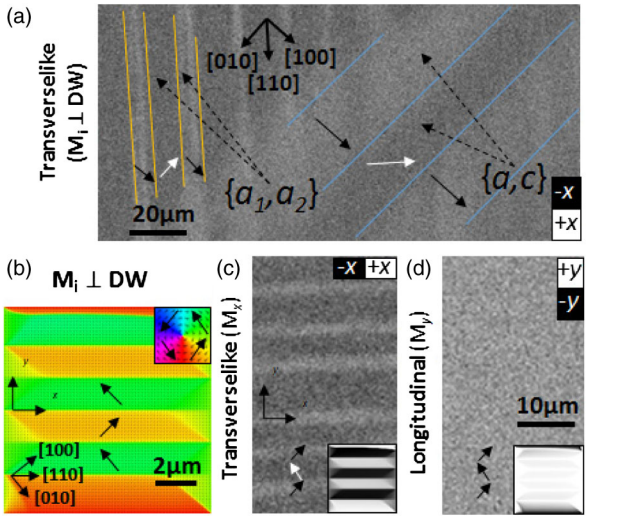

FIG. 2. (a) Transverselike MOKE image of the remanent state taken with initial magnetic saturated state parallel to the $\{a_1, a_2\}$ domain walls ($M_i \perp$DW). This image reveals the presence of both $\{a, c\}$ and $\{a_1, a_2\}$ domains. (b) Micromagnetic simulation of the remanent state for DW. (c) Transverse and (d) longitudinal MOKE remanence images for $M_i \perp$DW. The insets of (c) and (d) show, respectively, the x and y projections of the magnetization (M_x, M_y) as obtained from the micromagnetic simulations. In all panels the arrows indicate the orientation of the magnetization. The inset in (b) shows the color code for the direction of the magnetization.

To visualize simultaneously both types of twins, we perform Magneto-optical Kerr effect (MOKE) imaging of a 50-nm-thick CoFeB film grown on $SrTiO_3$. In this structure, similarly to the previously reported imprinting of ferroelastic domains into a magnetostrictive film on $BaTiO_3$ [28,29], the strain transfer from ferroelastic twins causes a modulation of the magnetic anisotropy via inverse magnetostriction. Here we use such magnetoelastic coupling to reveal the presence of $\{a, c\}$ and $\{a_1, a_2\}$ twins running along the [010] and [110] directions, respectively [Fig. 2(a)]. For that purpose, MOKE imaging is performed in the remnant state, after applying a magnetic field to set the initial magnetic saturated states of the CoFeB layer perpendicular to the ferroelastic domain walls ($M_i \perp$DW). In this magnetic configuration, we performed micromagnetic simulations that predict the formation of head-to-tail domains that perfectly match the underlying structure of $\{a_1, a_2\}$ twins [Fig. 2(b)] [30]. This observation is confirmed by MOKE images taken in transverselike and longitudinal configurations which, for $M_i \perp$DW, are sensitive, respectively, to the x and y projections of the magnetization [Figs. 2(c) and 2(d)].

In view of these results, we use transverselike MOKE imaging with $M_i \perp$DW to reveal the ferroelastic domain structure under electric fields. For instance, images recorded over a large area (~ 0.15 mm^2) at $V = -200, 0$, and $+200$ V show the collapse of $\{a, c\}$ domains after the application of out-of-plane electric fields, while $\{a_1, a_2\}$ twins expand [Fig. 3(a)]. This conclusion is consistent with the recession of $\{a, c\}$ twins observed by the optical images shown in Fig. 1, and is further corroborated by optical reflectance images taken *simultaneously* with the MOKE images shown in Fig. 3(a). Note that, as discussed above, reflectance imaging only reveals the surface topography and therefore is insensitive to the redistribution of $\{a_1, a_2\}$ twins. Thus, by subtracting the optical images recorded at different electric fields (i.e., $I_{V=0} - I_{V=+200\text{ V}}$ and $I_{V=0} - I_{V=-200\text{ V}}$), we disclose the areas in which $\{a, c\}$ twins are suppressed and replaced by $\{a_1, a_2\}$ domains, as shown in the slanted striped contrast in Fig. 3(b).

We will now discuss the effect of temperature on the distribution of ferroelastic twins. For that purpose, we select a region [(length) ≈ 400 μm $\times$ (width) ≈ 20 μm] perpendicular to the $\{a_1, a_2\}$ domain walls. At each position along the length, the MOKE intensity is averaged over the width of the selected area. This operation is repeated as a function of the magnetic field strength, thus obtaining a visualization of the magnetization direction at every point along the normal to the $\{a_1, a_2\}$ walls and at each magnetic field of the increasing hysteresis branch (from -8 to $+8$ mT); see Fig. S4 (Supplemental Material) [35]. Using this procedure we could visualize the effect of the emergence of ferroelastic twins on the magnetization reversal of the CoFeB film. For instance, at $T = 8$ K the presence of $\{a_1, a_2\}$ twins is already visible at $V = 0$ V [Fig. S4(a) in Ref. [35]]. After the application of a voltage $V = +200$ V, the number of $\{a_1, a_2\}$ twins increases,

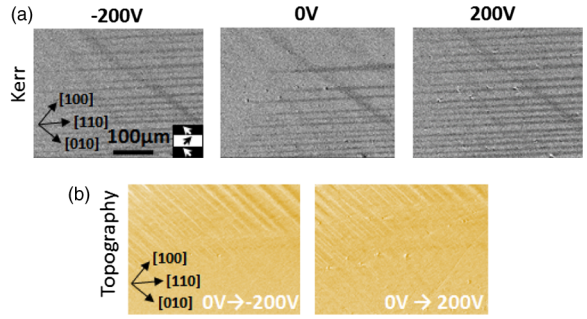

FIG. 3. (a) Transverse MOKE images of the remanent magnetic state ($M_i \perp$DW) at $V = -200$, 0, $+200$ V. The horizontal stripes indicate $\{a_1, a_2\}$ twins. (b) Images obtained after subtraction of the optical images taken simultaneously with MOKE images shown in (a). The left-hand image in (b) was obtained by subtracting the data at $V = 0$ V from that at $V = -200$ V ($I_{V=0} - I_{V=-200\ \mathrm{V}}$) and the right-hand image by subtracting data at $V = 0$ V from that at $V = +200$ V ($I_{V=0} - I_{V=+200\ \mathrm{V}}$). Thus, images in (b) indicate the areas where $\{a, c\}$ twins were suppressed by the electric field.

while the application of higher voltages ($V = +300$ V) has no further effect [Fig. S4(a) [35]]. By contrast, when the temperature rises, higher electric fields are needed to increase the number of $\{a_1, a_2\}$ twins. This is shown in Fig. S4(b) [35], which shows images recorded at $T = 50$ K. At $V = +200$ V, the $\{a_1, a_2\}$ twins grow, but the effect is not saturated, since higher voltages ($V = +300$ V) are needed to expand further $\{a_1, a_2\}$ domains. Therefore, as temperature increases towards the transition, the electric-field-induced motion of twins becomes stiffer.

Summing up, the application of an out-of-plane electric field expands $\{a_1, a_2\}$ twins—i.e., domains with both elongated axes in the plane—at the expense of $\{a, c\}$ twins. This conclusion is also confirmed by optical birefringence images taken in transmission (Fig. S3 in the Supplemental Material [35]). To explain this result, various hypotheses are possible. As we said in the introduction, it is natural to expect an electrical bias to couple with the intrinsic polarity of the walls, and hence determine their motion. In our case, however, we can safely rule out such a mechanism as the main driving force. Indeed, the domain wall polarity (P) is oriented, by symmetry, towards the apex of the twin [37]; this implies [Fig. 1(a)] that only $\{a, c\}$ twin walls can have a nonzero out-of-plane component of P and, hence, couple to a (001) field. Thus, domain wall polarity alone would promote an expansion of the $\{a, c\}$ regions at the expense of the $\{a_1, a_2\}$ ones, which is the exact opposite of what we observe. Additionally, as shown in Fig. S4 (Supplemental Material) [35], electric fields still promote the emergence of $\{a_1, a_2\}$ domains even at temperatures where evidence of the domain wall polarity is weak [16].

Since the properties of the walls cannot explain our observations, the answer must lie within the domains. The most likely candidate in this context is the dielectric anisotropy of tetragonal $SrTiO_3$. To see the relationship between the domain structure and the dielectric anisotropy, consider the electrostatic enthalpy of a parallel-plate capacitor $\mathcal{F}(E_f) = -\Omega(\epsilon_0\epsilon/2)E_f^2$, where Ω is the volume of the dielectric, ϵ_0 and ϵ are its vacuum and relative permittivity, and E_f is the electric field. A larger value of ϵ implies an energy gain and, thus, domains with higher polarizability along the applied electric field are favored. As we show in the following, the polarizability is significantly larger along the normal to the AFD tilt axis. This implies that a-type domains are energetically favored under an applied electric field, which nicely fits with the experimentally observed expansion of the $\{a_1, a_2\}$ regions.

We consider the following Landau-type energy expansion around the parent cubic phase:

$$E = \frac{C_{\alpha\beta}}{2}\varepsilon_\alpha\varepsilon_\beta + \frac{A}{2}|\phi|^2 + B|\phi|^4 - R_{ii\alpha}\phi_i^2\varepsilon_\alpha + \frac{\chi_0^{-1}}{2}|P|^2 - Q_{iijj}\phi_i^2P_j^2 - e_{ii\alpha}P_i^2\varepsilon_\alpha + \frac{\beta}{2}|u^{Ti}|^2 + N\epsilon_{ijk}P_iu_j^{Ti}\phi_k. \quad (1)$$

Equation (1) includes the standard couplings that are typically considered in the literature: the elastic energy ($C_{\alpha\beta}$ is the elastic tensor), the double-well potential (A and B) associated to octahedral tilts (ϕ_k), the "rotostriction" ($R_{ii\alpha}$) between oxygen tilts and the tetragonal strain, the harmonic energy associated with the "soft" polar mode (χ_0^{-1} is the inverse of its contribution to the dielectric susceptibility), the biquadratic coupling between the polar mode and oxygen tilts (Q_{iijj}), and electrostriction ($e_{ii\alpha}$). The last two terms describe a previously overlooked trilinear coupling mechanism that involves, in addition to the polarization and the tilts, an antiferroelectric mode of the Ti atoms, (u_j^{Ti}) [see the schematic lattice representation in Fig. 4(a)]. Such a coupling (N is a scalar and ϵ_{ijk} is the antisymmetric Levi-Civita tensor) implies that P and u_j^{Ti} can mix in the ferroelastic tetragonal phase, leading to a "softening" of the polar mode [38] and to the IR activity of the AFE u_j^{Ti} mode. As we shall see shortly, both effects have important implications.

To quantify the impact of Eq. (1) on the energetics of the crystal, we study the inverse dielectric constant ϵ^{-1}, which in $SrTiO_3$ can be very well approximated [$\epsilon^{-1} \sim (\epsilon - 1)^{-1}$] by taking the second derivative of the energy with respect to the polarization:

$$4\pi\epsilon^{-1} \sim \frac{d^2E}{dP_i^2} = \chi_0^{-1}(T) - 2\sum_k \tilde{Q}_{kkii}\phi_k^2(T). \quad (2)$$

Here, $\tilde{Q}_{kkii}$ is an effective biquadratic coupling tensor that includes the contribution of strain and the antiferroelectric mode [see the Supplemental Material for the derivation of Eq. (3)] [39]:

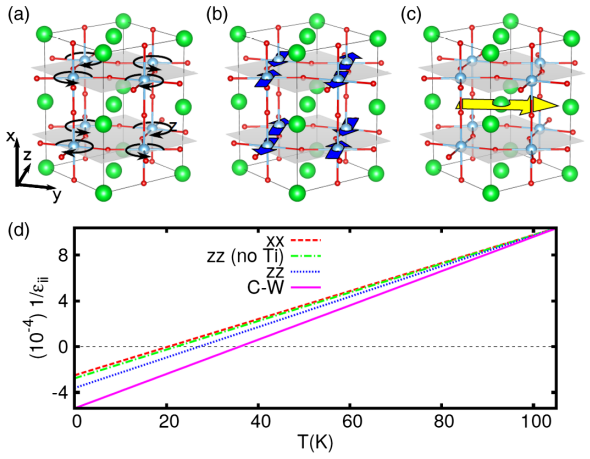

FIG. 4. Panels (a) and (b) show schematically the three modes that are coupled by the trilinear term in Eq. (1). (a) AFD mode along the x axis, (b) AFE mode of the Ti atoms along the z axis, and (c) polar mode along the y direction. The yellow arrow in (c) indicates the direction of the polar mode. (d) Inverse dielectric constant ϵ_{ii}^{-1} as function of temperature. The pink dashed line is the Curie-Weiss (labeled C-W) law fitted by experimental data at high temperature, and represents the expected behavior if the crystal remained in the cubic high-symmetry structure. The red (labeled as xx) and the blue (zz) lines are the calculated values for ϵ_{xx}^{-1} (out of plane) and ϵ_{zz}^{-1} (in plane), respectively. For comparison, we also show ["zz (no Ti)," green dashed line] the hypothetical behavior of ϵ_{zz}^{-1} if we suppressed the trilinear coupling to the antiferroelectric-Ti mode.

$$\tilde{Q}_{kkii} = Q_{kkii} + e_{kk\alpha}C^{-1}_{\alpha\beta}R_{ii\beta} + \frac{N^2}{2\beta}(1-\delta_{ik}). \qquad (3)$$

In Eq. (2), the term $\chi_0^{-1}(T)$ reproduces the experimental Curie-Weiss behavior of the inverse dielectric susceptibility and $\phi_k^2(T)$ accounts for the temperature dependence of the octahedral tilts. Given the cubic symmetry and the nature of the spontaneous distortion, only two components of $\tilde{Q}_{kkii}$ are relevant to our study, namely, the longitudinal $\tilde{Q}_{1111}$ and transverse $\tilde{Q}_{1122}$ components.

We are now in a position to determine the specific contributions of strain, tilts, and the antiferroelectric mode to the dielectric behavior of $SrTiO_3$. For that purpose, we calculate all coefficients in Eq. (1) by following the strategy outlined in Ref. [42], i.e., employing density functional perturbation theory, and using the local-density approximation and norm-conserving pseudopotentials [48]. As a first step, we consider only the first two terms in Eq. (3), i.e., excluding the antiferroelectric mode. In these conditions, we find that the values for the longitudinal and transverse components of Q_{kkii} and $Q^{(e)}_{kkii} = e_{kk\alpha}C^{-1}_{\alpha\beta}R_{ii\beta}$ are similar ($\tilde{Q}_{1111}=Q_{1111}+Q^{(e)}_{1111}=-0.113$, $\tilde{Q}_{1122} = Q_{1122} + Q^{(e)}_{1122} = -0.103$, see Table I) and, thus, the calculated dielectric constant is nearly isotropic. Although such values do indicate a relative softening of the dielectric response normal to the octahedral tilt axis, the inferred anisotropy seems too weak to account for the observed field-induced ferroelastic twin redistributions. Without considering u_j^{Ti}, the calculated values of ϵ_{xx}^{-1} and ϵ_{zz}^{-1} are virtually the same at any temperature [see the red dashed and green dash-dotted lines in Fig. 4(b)].

TABLE I. Values calculated for the coefficients Q_{kkii}, $Q^{(e)}_{kkii}$, $Q^{(Ti)}_{kkii}$ defined in the text. Ha/bohr units are used.

	Q_{kkii}	$Q^{(e)}_{kkii}$	$Q^{(Ti)}_{kkii}$
1111	−0.208	+0.095	⋯
1122	−0.031	−0.072	0.033

It turns out that the antiferroelectric u_j^{Ti} mode provides a crucial contribution to the dielectric anisotropy. To understand why, note that $Q^{(\mathrm{Ti})}_{ik} = (N^2/2\beta)(1-\delta_{ik})$ in Eq. (3) is defined positive, and only affects the transverse $\tilde{Q}_{1122}$ component. Thus, $Q^{(\mathrm{Ti})}_{ik}$ leads to a further, pronounced *softening* of the components of the dielectric tensor that are normal to the AFD tilt axis. Indeed, the calculated value is $Q^{(Ti)}_{ik} = 0.033$, so that $\tilde{Q}_{1122} = Q_{1122} + Q^{(e)}_{1122} + Q^{(\mathrm{Ti})}_{1122} = -0.070$; this is significantly smaller than $\tilde{Q}_{1111} = -0.113$ (see Table I). As a result, the final values of the out-of-plane ϵ_{xx}^{-1} and in-plane ϵ_{zz}^{-1} components [red dashed and blue dotted lines in Fig. 4(b)] clearly differ. Our conclusions on the dielectric anisotropy are in good agreement with the available experimental literature [7,47,49] and earlier theoretical studies [38]. Also, the fast decrease of the dielectric susceptibility of $SrTiO_3$ with temperature and the ensuing reduction of polarizability is likely responsible for the increasingly hindered ferroelastic twin motion as the transition temperature is approached (see Fig. S4 in Supplemental Material) [35].

Now we turn to the question of the origin of the IR-active R phonon. Our theory predicts that the antiferroelectric u_j^{Ti} vibration occurs at a frequency $\omega \sim 440$ cm^{-1}. Remarkably, an R mode with E_u symmetry, the same as u_j^{Ti}, see Fig. 4(a), was observed [25] at a frequency $\omega \sim 435$ cm^{-1}, essentially matching our prediction. Such an R mode was tentatively assigned to the doubling of the unit cell and subsequent backfolding of phonon modes from the boundary to the center of the Brillouin zone [26,27]. Clearly, our combined experimental and theoretical analysis allows us to unambiguously identify such an R mode with the antiferroelectric u_j^{Ti} phonon described in our work. Note that this mode plays a significant role in the physics of $SrTiO_3$ at low temperatures, as it also mediates an important contribution to the polarity of the twin walls [37].

Before closing, it is worth noting that our model [Eqs. (1)–(3)] also predicts the appearance of dielectric anomalies across the ferroelastic transition associated with the interplay of AFD, polar, and AFE lattice instabilities.

Such couplings should lead to measurable deviations from the Curie-Weiss behavior of $SrTiO_3$ (in addition to the well-known deviations that are due to the "quantum paraelectric" regime) below the ferroelastic transition. We regard this as an interesting topic for future studies.

We acknowledge the support of Ministerio de Economía, Industria y Competitividad (MINECO-Spain) through Grants No. MAT2017-85232-R, No. MAT2014-56063-C2-1-R, No. MAT2016-77100-C2-2-P, No. FIS2013-48668-C2-2-P, and Severo Ochoa SEV-2015-0496, the Generalitat de Catalunya through Grants No. 2017 SGR1377 and No. 2017 SGR1506, the Väisälä foundation and the STSM Grant from the COST Action MP1308. This project has received funding from the European Research Council (ERC) under the European Union's Horizon 2020 research and innovation programme (Grant Agreements No. 724529 and No. 307502). Calculations were performed at Supercomputing Center of Galicia (CESGA).

[1] T. Wolfram and S. Ellialtoglu, *Electronic and Optical Properties of d-Band Perovskites* (Cambridge University Press, Cambridge, England, 2006).

[2] R. A. Cowley, The phase transition of strontium titanate, Phil. Trans. R. Soc. A **354**, 2799 (1996).

[3] F. W. Lytle, X-ray diffractometry of low-temperature phase transformations in strontium titanate, J. Appl. Phys. **35**, 2212 (1964).

[4] A. V. Kityk, W. Schranz, P. Sondergeld, D. Havlik, E. K. H. Salje, and J. F. Scott, Low-frequency superelasticity and nonlinear elastic behavior of $SrTiO_3$ crystals, Phys. Rev. B **61**, 946 (2000).

[5] J. Slonczewand H. Thomas Interaction of elastic strain with structural transition of strontium titanate, Phys. Rev. B **1**, 3599 (1970).

[6] K. A. Müller and H. Burkard, An intrinsic quantum paraelectric below 4 K, Phys. Rev. B **19**, 3593 (1979).

[7] T. Sakudo and H. Unoki, Dielectric Properties of $SrTiO_3$ at Low Temperatures, Phys. Rev. Lett. **26**, 851 (1971).

[8] E. Courtens, Birefringence of $SrTiO_3$ Produced by the 105 K Structural Phase Transition, Phys. Rev. Lett. **29**, 1380 (1972).

[9] B. Kalisky *et al.*, Locally enhanced conductivity due to the tetragonal domain structure in $LaAlO_3/SrTiO_3$ heterointerfaces, Nat. Mater. **12**, 1091 (2013).

[10] M. Honig, J. A. Sulpizio, J. Drori, A. Joshua, E. Zeldov, and S. Ilani, Local electrostatic imaging of striped domain order in $LaAlO_3/SrTiO_3$, Nat. Mater. **12**, 1112 (2013).

[11] Y. Frenkel, N. Haham, Y. Shperber, C. Bell, Y. Xie, Z. Chen, Y. Hikita, H. Y. Hwang, and B. Kalisky, Anisotropic transport at the $LaAlO_3/SrTiO_3$ interface explained by microscopic imaging of channel-flow over $SrTiO_3$ domains, ACS Appl. Mater. Interfaces **8**, 12514 (2016).

[12] X. Lin, Z. Zhu, B. Fauqué, and K. Behnia, Fermi Surface of the Most Dilute Superconductor, Phys. Rev. X **3**, 021002 (2013).

[13] A. Santander-Syro *et al.* Two-dimensional electron gas with universal subbands at the surface of $SrTiO_3$, Nature (London) **469**, 189 (2011).

[14] A. Ohtomo and H. Y. Hwang, A high-mobility electron gas at the $LaAlO_3/SrTiO_3$ heterointerface, Nature (London) **427**, 423 (2004).

[15] Y. Z. Chen, N. Bovet, F. Trier, D. V. Christensen, F. M. Qu, N. H. Andersen, T. Kasama, W. Zhang, R. Giraud, J. Dufouleur, T. S. Jespersen, J. R. Sun, A. Smith, J. Nygård, L. Lu, B. Büchner, B. G. Shen, S. Linderoth, and N. Pryds, A high-mobility two-dimensional electron gas at the spinel/perovskite interface of γ-$Al_2O_3/SrTiO_3$, Nat. Commun. **4**, 1371 (2013).

[16] E. K. H. Salje, O. Aktas, M. A. Carpenter, V. V. Laguta, and J. F. Scott, Domains Within Domains and Walls Within Walls: Evidence for Polar Domains in Cryogenic $SrTiO_3$, Phys. Rev. Lett. **111**, 247603 (2013).

[17] E. K. H. Salje and J. F. Scott, Ferroelectric Bloch-line switching: A paradigm for memory devices?, Appl. Phys. Lett. **105**, 252904 (2014).

[18] J. Hemberger, P. Lunkenheimer, R. Viana, R. Bohmer, and A. Loidl, Electric-field-dependent dielectric-constant and nonlinear susceptibility in $SrTiO_3$, Phys. Rev. B **52**, 13159 (1995).

[19] P. Zubko, G. Catalan, A. Buckley, P. R. L. Welche, and J. F. Scott, Strain-Gradient-Induced Polarization in $SrTiO_3$ Single Crystals, Phys. Rev. Lett. **99**, 167601 (2007).

[20] J. F. Scott, E. K. H. Salje, and M. A. Carpenter, Domain Wall Damping and Elastic Softening in $SrTiO_3$: Evidence for Polar Twin Walls, Phys. Rev. Lett. **109**, 187601 (2012).

[21] H. J. Harsan Ma *et al.*, Local Electrical Imaging of Tetragonal Domains and Field-Induced Ferroelectric Twin Walls in Conducting $SrTiO_3$, Phys. Rev. Lett. **116**, 257601 (2016).

[22] Y. Frenkel, N. Haham, Y. Shperber, C. Bell, Y. Xie, Z. Chen, Y. Hikita, H. Y. Hwang, E. K. H. Salje, and B. Kalisky, Imaging and tuning polarity at $SrTiO_3$ domain walls, Nat. Mater. **16**, 1203 (2017).

[23] V. K. Vlasko-Vlasov, Y. K. Lin, D. J. Miller, U. Welp, G. W. Crabtree, and V. I. Nikitenko, Direct Magneto-Optical Observation of a Structural Phase Transition in Thin Films of Manganites, Phys. Rev. Lett. **84**, 2239 (2000).

[24] Z. Erlich *et al.*, Optical study of tetragonal domains in $LaAlO_3/SrTiO_3$, J. Supercond. Novel Magn. **28**, 1017 (2015).

[25] J. Petzelt, T. Ostapchuk, I. Gregora, I. Rychetsky, S. Hoffmann-Eifert, A. V. Pronin, Y. Yuzyuk, B. P. Gorshunov, S. Kamba, V. Bovtun, J. Pokorny, M. Savinov, V. Porokhonskyy, D. Rafaja, P. Vanek, A. Almeida, M. R. Chaves, A. A. Volkov, M. Dressel, and R. Waser, Dielectric, infrared, and Raman response of undoped $SrTiO_3$ ceramics: Evidence of polar grain boundaries, Phys. Rev. B **64**, 184111 (2001).

[26] M. Yazdi-Rizi, P. Marsik, B. P. P. Mallett, and C. Bernhard, Anisotropy of infrared-active phonon modes in the monodomain state of tetragonal $SrTiO_3$ (110), Phys. Rev. B **95**, 024105 (2017).

[27] P. A. Fleury, J. F. Scott, and J. M. Worlock, Soft Phonon Modes and the 110 °K Phase Transition in $SrTiO_3$, Phys. Rev. Lett. **21**, 16 (1968).

[28] T. H. E. Lahtinen, J. O. Tuomi, and S. van Dijken, Pattern transfer, and electric-field-induced magnetic domain formation in multiferroic heterostructures, Adv. Mater. **23**, 3187 (2011).

[29] T. H. E. Lahtinen, K. J. A. Franke, and S. van Dijken, Electric-field control of magnetic domain wall motion, and local magnetization reversal, Sci. Rep. **2**, 258 (2012).

[30] See Supplemental Material at http://link.aps.org/supplemental/10.1103/PhysRevLett.120.217601 for more details on the micromagnetic simulations, which includes Refs. [31–34].

[31] R. Loetzsch, A. Lübcke, I. Uschmann, E. Förster, V. Große, M. Thuerk, T. Koettig, F. Schmidl, and P. Seidel, The cubic to tetragonal phase transition in $SrTiO_3$ single crystals near its surface under internal and external strains, Appl. Phys. Lett. **96**, 071901 (2010).

[32] B. D. Cullity and C. D. Graham, *Introduction to Magnetic Materials* (John Wiley & Sons, New York, 2011).

[33] D. Wang, C. Nordman, Z. Qian, J. M. Daughton, and J. Myers, Magnetostriction effect of amorphous CoFeB thin films and application in spin-dependent tunnel junctions, J. Appl. Phys. **97**, 10C906 (2005).

[34] S. Zhang *et al.*, Giant electrical modulation of magnetization in $Co_{40}Fe_{40}B_{20}/Pb(Mg_{1/3}Nb_{2/3})_{0.7}Ti_{0.3}O_3(011)$ heterostructure, Sci. Rep. **4**, 3727 (2014).

[35] See Supplemental Material at http://link.aps.org/supplemental/10.1103/PhysRevLett.120.217601 for the temperature dependence of the electric-field-induced distribution of ferroelastic domains, which includes Ref. [36].

[36] A. Casiraghi, T. R. Domínguez, S. Rößler, K. J. A. Franke, D. L. González, S. J. Hämäläinen, R. Frömter, H. P. Oepen, and S. van Dijken, Influence of elastically pinned magnetic domain walls on magnetization reversal in multiferroic heterostructures, Phys. Rev. B **92**, 054406 (2015).

[37] A. Schiaffino and M. Stengel, Macroscopic Polarization from Antiferrodistortive Cycloids in Ferroelastic $SrTiO_3$, Phys. Rev. Lett. **119**, 137601 (2017).

[38] N. Sai and D. Vanderbilt, First-principles study of ferroelectric and antiferrodistortive instabilities in tetragonal $SrTiO_3$, Phys. Rev. B **62**, 13942 (2000).

[39] See Supplemental Material at http://link.aps.org/supplemental/10.1103/PhysRevLett.120.217601 for computational methods, which includes Refs. [38,40–47].

[40] X. Gonze *et al.*, ABINIT: First-principles approach to material and nanosystem properties, Comput. Phys. Commun. **180**, 2582 (2009).

[41] N. Troullier and J. L. Martins, Efficient pseudopotentials for plane-wave calculations, Phys. Rev. B **43**, 1993 (1991).

[42] M. Stengel, Unified *ab initio* formulation of flexoelectricity and strain-gradient elasticity, Phys. Rev. B **93**, 245107 (2016).

[43] X. Gonze, First-principles responses of solids to atomic displacements, and homogeneous electric fields: Implementation of a conjugate-gradient algorithm, Phys. Rev. B **55**, 10337 (1997).

[44] X. Gonze and C. Lee, Dynamical matrices, Born effective charges, dielectric permittivity tensors, and interatomic force constants from density-functional perturbation theory, Phys. Rev. B **55**, 10355 (1997).

[45] S. Baroni, S. de Gironcoli, and A. Dal Corso, phonons and related crystal properties from density-functional perturbation theory, Rev. Mod. Phys. **73**, 515 (2001).

[46] A. K. Tagantsev, E. Courtens, and L. Arzel, Prediction of a low-temperature ferroelectric instability in antiphase domain boundaries of strontium titanate, Phys. Rev. B **64**, 224107 (2001).

[47] H. Uwe and T. Sakudo, Stress-induced ferroelectricity and soft phonon modes in $SrTiO_3$, Phys. Rev. B **13**, 271 (1976).

[48] All the simulations have been performed within the local-density approximation and using norm-conserving pseudopotentials, treating explicitly 10 electrons for Sr, 12 for Ti, and 6 for O. Monkhorst-Pack $6 \times 6 \times 6$ and cutoff 70 Ha.

[49] B. Pietrass, Field-induced switching of tetragonal domains in $SrTiO_3$ at low temperatures, Phys. Status Solidi (a) **9**, K39 (1972).